Supplemental Material

EXCITON MODEL

To rationalize the pump probe SFG spectra of Fig. 2c we constructed a model based on first-order perturbation calculations to determine the vibrational excitonic states (vibrons) arising from the electric dipole-dipole coupling between the CO molecules in the monolayer [1-3]. We used the Frenkel-exciton Hamiltonian [4] for coupled anharmonic oscillators to define the perturbation matrix for the different exciton manifolds which, after diagonalization gives for each manifold, the exciton energies and wave functions from which the IR transition energies and integrated cross-sections are determined.

To limit the computational costs, the calculations were performed for ($N =$) 9 CO molecules bound via the carbon atom perpendicular to the Au surface on a hexagonal 3x3 grid. Hence, the site basis for the system is

$$\{|v_1\rangle, |v_2\rangle, \dots |v_9\rangle\}$$

where the state vector elements correspond to the vibrational quantum states of the nine individual unperturbed CO molecules. The unperturbed ground state in this basis is: $E_0' = |0,0,0,0,0,0,0,0,0\rangle$, where the index 0 indicates the zero-exciton manifold and the prime stands for the unperturbed states.

The IR_{pump} is in resonance with the 0→1 transition and can populate only CO(v=1) states. However, its intensity is high enough to deposit $i \leq N$ quanta into the system by resonant multi-photon absorption reaching the i^{th}-exciton manifold. If we neglect CO-CO interactions, the states populated after one-, two-, three photon absorption events are as follows.

$$E_1' = \{|1,0,0,0,0,0,0,0,0\rangle, |0,1,0,0,0,0,0,0,0\rangle, \dots |0,0,0,0,0,0,0,0,1\rangle\} \quad \text{(A1)}$$

$$E_2' = \{|1,1,0,0,0,0,0,0,0\rangle, \dots |1,0,0,0,0,0,0,0,1\rangle, |0,1,1,0,0,0,0,0,0\rangle, \dots |0,1,0,0,0,0,0,0,1\rangle, \dots\} \quad \text{(A2)}$$

$$E_3' = \{|1,1,1,0,0,0,0,0,0\rangle, \dots |1,1,0,0,0,0,0,0,1\rangle, |1,0,1,1,0,0,0,0,0\rangle, \dots |1,0,1,0,0,0,0,0,1\rangle, \dots\} \quad \text{(A3)}$$

$$\vdots$$

$$E_i' = \{\dots\}$$

States with higher excitation can be obtained in a similar way. Each unperturbed exciton manifold consists of N_i states corresponding to the number of permutations the i vibrational quanta can be distributed over the N molecules:

$$N_i = \frac{N!}{(N-i)! \cdot i!} \quad \text{(A4)}$$

The IR_{probe} moves population to the next higher exciton manifold $j=i+1$ and due to its tunable frequency, may induce either 0→1 or 1→2 transitions, the latter being anharmonically red-shifted from the former. We emphasize that the probe laser's intensity is so low that only one-photon absorption occurs. Hence, the exciton-manifold accessible after IR_{probe}-photon absorption consist of the following unperturbed states:

$$F_2' = \left\{ \begin{matrix} |2,0,0,0,0,0,0,0,0\rangle, |0,2,0,0,0,0,0,0,0\rangle, \dots |0,0,0,0,0,0,0,0,2\rangle, \\ |1,1,0,0,0,0,0,0,0\rangle, \dots |1,0,0,0,0,0,0,0,1\rangle, |0,1,1,0,0,0,0,0,0\rangle, \dots |0,1,0,0,0,0,0,0,1\rangle, \dots \end{matrix} \right\} \quad \text{(A5)}$$

$$F_3' = \left\{ \begin{matrix} |2,1,0,0,0,0,0,0,0\rangle, \dots |2,0,0,0,0,0,0,0,1\rangle, |1,2,0,0,0,0,0,0,0\rangle \dots |0,2,0,0,0,0,0,0,1\rangle, \dots \\ |1,1,1,0,0,0,0,0,0\rangle, \dots |1,1,0,0,0,0,0,0,1\rangle, |1,0,1,1,0,0,0,0,0\rangle, \dots |1,0,1,0,0,0,0,0,1\rangle, \dots \end{matrix} \right\} \quad \text{(A6)}$$

$$\vdots$$

$$F_j' = \{\dots\}$$

derived from E_1' and E_2'. F_4' through F_9' would be found in an analogous way. These exciton manifolds are denoted by F_j' because they also contain doubly excited CO molecules (upper row in Eqs. (A5) and (A6), which can only be produced when the probe laser is tuned to the 1-2 transition). Here, each manifold consists of

$$N_j' = \frac{N!}{(N-j)!\cdot j!} + \frac{N!}{(N-(j-1))!\cdot (j-2)!} \quad \text{(A7)}$$

states.

In Table I (see next page) values for N_i and N_{i+1}' are shown for a system of nine CO molecules with various levels of vibrational excitation. For example, if ($i =$) four CO molecules are excited by IR_{pump}, the four-exciton manifold consists of ($N_{i=4} =$) 126 states. With the subsequent absorption of a probe-photon, a transition to the five-exciton-manifold with ($N_{i+1}' =$) 630 states takes place.

We next couple these states by dipole-dipole interactions using the perturbed Hamiltonian, $\underline{\boldsymbol{H}}^{(1)}$. The diagonal elements are given by

$$H_{kk}^{(1)} = \sum_{i=1}^{N} \epsilon_i + \sum_{i=1}^{N} \sum_{j<i}^{N} f_{ij}\, \mu^{(i)} \mu^{(j)} \quad \text{(A8)}$$

where ϵ_i, is the intrinsic excitation energy at site-i and the double summation represents the static dipole-dipole interaction for state-k, which must be summed over all pairs of interactions. The off-diagonal matrix elements of the perturbed Hamiltonian are

$$H_{nm}^{(1)} = f_{ij}\, \mu^{(i)} \mu^{(j)} \quad \text{(A9)}$$

***Table I**: Number of exciton states in pump and probe manifolds, and distinct IR transitions between them*

Number of CO molecules	N	**9**							
Number of CO v=1 quanta excited	i	1	2	3	4	5	6	7	8
No. of exciton states after pump pulse (Eq. A4)	N_i	9	36	84	126	126	84	36	9
No. of exciton states after probe pulse (Eq. A7)	N'_{i+1}	45	156	378	630	714	540	261	73
Probe resonant with 0-1 transition	$N_{0\to1}$	6	22	48	63	48	22	6	1
Probe resonant with 1-2 transition	$N_{1\to2}$	3	21	83	175	206	131	47	9

Where *n* and *m* refer to two coupled basis states in which two CO molecules *i* and *j* exchange one vibrational quantum. Accordingly, the dipole terms in (A9) are transition dipole moments μ^{01} or μ^{12}, dependent on whether 0↔1 or 1↔2 transitions are involved. Off-diagonal matrix elements requiring the exchange of more than one vibrational quantum in the site basis states are zero.

Anharmonicity is included in an *ad hoc* manner [5] by lowering the site energy of doubly excited site states by an energy Δ, twice the CO gas phase anharmonic constant. The dipole terms in Eq. (A8) are μ^{00}, μ^{11}, and μ^{22} for the permanent dipole moments averaged over the vibrational states *v* = 0, 1, and 2, respectively, and f_{ij} is given by

$$f_{ij} = \frac{1}{4\pi\varepsilon_0 {r_{ij}}^3} \quad , \tag{A10}$$

when CO molecules are oriented perpendicular to the surface, as is approximately the case in this system. Here, r_{ij} is the distance between sites *i* and *j*. Note, that the exciton coupling conserves the number of states in each manifold. For calculating the matrix elements we assume that the CO surface bond is so weak that it hardly affects the molecular properties; we then use dipole moment matrix elements for the gas phase molecule [6,7]:

$$\mu^{00} = \langle 0|\mu|0\rangle = -0.112\ D$$

$$\mu^{11} = \langle 1|\mu|1\rangle = -0.087\ D$$

$$\mu^{22} = \langle 2|\mu|2\rangle = -0.062\ D$$

$$\mu^{01} = \langle 0|\mu|1\rangle = 0.105\ D$$

$$\mu^{12} = \langle 1|\mu|2\rangle = \sqrt{2}\cdot\mu^{01}$$

The CO-CO distances in the 3x3 hexagonal grid are derived from the known structure of the monolayer at saturation coverage [8]; this leads us to a nearest neighbor distance of 5.77 Å. We applied periodic boundary conditions for calculating the dipole-dipole coupling energies and used the unperturbed 0→1 energy ($\tilde{\nu}_0 = 2129.6$ cm^{-1}) and the anharmonic shift $\Delta = 26$ cm^{-1} as adjustable parameters.

Diagonalization of the perturbed Hamiltonian results in exciton states ψ_n and ψ_m distributed among manifolds E_i and F_j. The resulting eigenenergies ε_m(in manifold F_j) and ε_n (in manifold E_i) determine the IR transition frequencies:

$$\tilde{\nu}_{mn} = \frac{\varepsilon_m - \varepsilon_n}{hc} \qquad \text{(A11)}.$$

The integrated cross-sections $\bar{\sigma}_{mn}$ (in units cm/molecule) are given by [1]:

$$\bar{\sigma}_{mn} = \frac{8\pi^3\tilde{\nu}_{mn}}{Nhc}\left|\sum_{j=1}^{N}\langle\psi_m|\mu_j|\psi_n\rangle\right|^2 \qquad \text{(A12)}$$

where the sum is over all CO molecules j.

Due to selection rules and degeneracies, the number of allowed and distinct IR transitions is much lower than the number of exciton states involved. An example is schematically shown in Fig. A1 for the IR transitions from E_4 to F_5, consisting of 126 and 630 exciton states, respectively. 63 v=0→1 transitions and 175 v=1→2 transitions exist between these two manifolds. See table AI.

Figure A2a shows stick spectra obtained with this model. We have color coded the manifold-dependent contributions. Note that the intensities of degenerate transitions were summed up. The spectra divide themselves into two well resolved features separated by the anharmonic shift Δ. Each feature exhibits a width ($\lesssim 2$ cm^{-1}) reflecting the energy dispersion of the states in the different manifolds influenced by dipole-dipole coupling. States containing one or more CO(v=1) barely mix with those containing a CO(v=2).

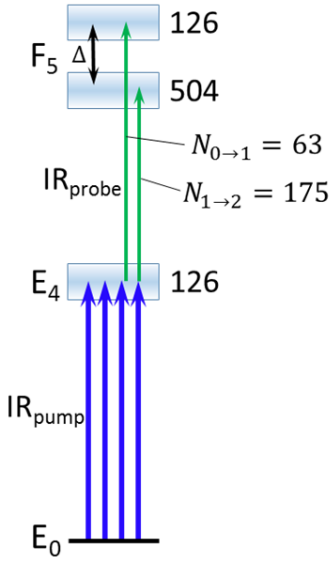

Figure A1. Allowed and distinct IR transitions (green arrows) from the exciton manifold E_4 to the manifold F_5.

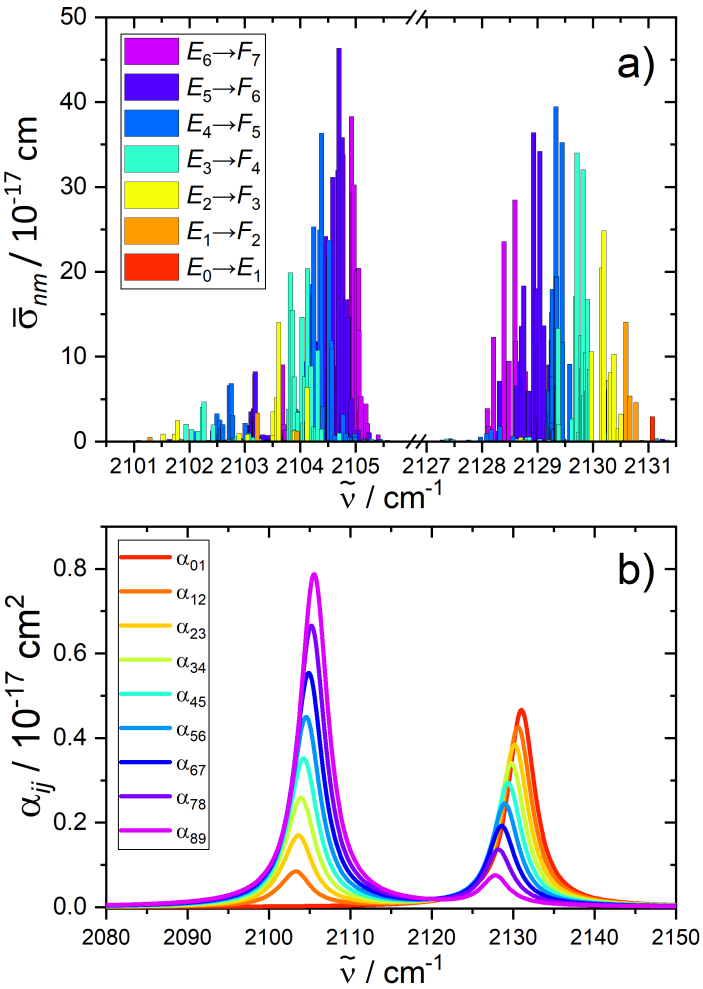

Figure A2. a) Integrated absorption cross sections for individual exciton transitions between manifolds i and i+1, respectively (the intensities of degenerate transitions were summed up, note the break in the frequency axis); b) simulated average absorption cross section for transition between exciton manifolds i and i+1 assuming a Lorentzian lineshape of 4 cm^{-1} FWHM.

We note that within this model, the IR transition frequencies exhibit a red-shift of the 0→1 feature and a blue-shift of the 1→2 feature with increasing excitation density. There is an additional factor we must consider to simulate experimental spectra. If a certain exciton manifold, E_i, is populated by IR_{pump}, there must be a fast redistribution of population between nearly degenerate states during the pump laser pulse. Hence, the occupancy of that state and the transition probability to a state in F_{i+1} will drop by a factor $1/N_i$ (see Eq. (A4)). Multiplying the intensities of Fig. A2a by $1/N_i$ and convoluting each transition with a Lorentzian line shape function of 4 cm^{-1} FWHM yields the averaged absorbance spectra α_{ij} shown in Fig. A2b. We note that the oscillator strength for the 1→2 absorption derived in this way is twice as strong as the 0→1 oscillator strength, providing us some confidence in the realistic nature of our model.

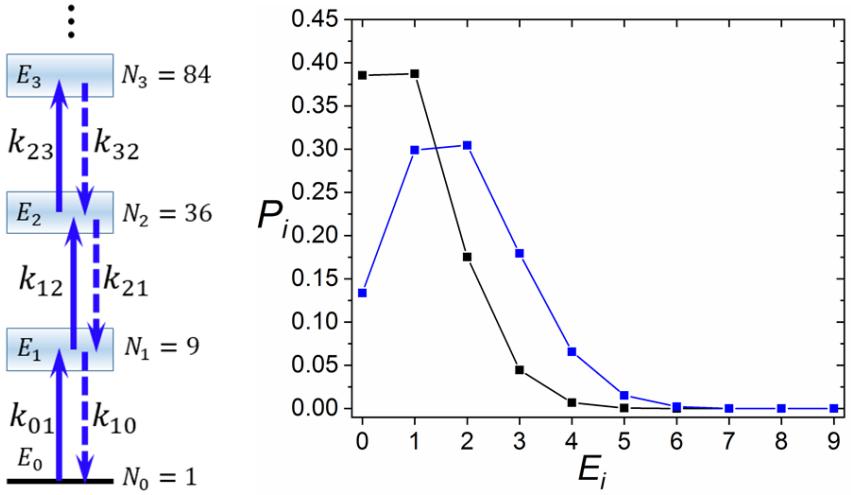

Figure A3. Left: Kinetic model describing the multi-photon absorption process by the IR pump pulse (upward and downward arrows indicate absorption and stimulated emission, respectively). Right: Fractional populations P_i in the manifolds E_i created with the kinetic model using pump fluences of 0.014 (black) and 0.031 J/cm^2 (blue), respectively. The insert shows the ratio P_i/N_i vs. E_i; The ensemble averaged population in the CO(v=1) state of the black and blue distributions are 10 and 20%, respectively.

To model the exciton distribution created by IR_{pump}, we assume a ladder climbing mechanism based on simple population kinetics ignoring coherence. The CO/Au(111) absorption line (Fig. 2) shows a width of $\Delta\tilde{\nu} = 6.5\, cm^{-1}$ corresponding to a dephasing time of $T_2 = (2\pi\, c \cdot \Delta\tilde{\nu})^{-1} = 0.8\, ps$. We assume this to be the timescale for energy redistribution within an exciton manifold E_i. Since the IR laser pulse width is 20 ps, energy redistribution is completed before higher exciton states are populated by absorption of additional pump photons. The kinetic model emerging from these considerations is shown in the left panel of Fig. A3, where the coupled differential equations describing the pumping process are

$$\frac{d\,E_0}{dt} = -k_{01}E_0 + k_{10}E_1 \qquad \text{(A13a)}$$

$$\frac{d\,E_1}{dt} = k_{01}E_0 - k_{10}E_1 - k_{12}E_1 + k_{21}E_2 \qquad \text{(A13b)}$$

etc.

Eqs. (A13) include absorption and stimulated emission induced by the laser field. The corresponding rate constants $k_{ij} = \alpha_{ij}(\tilde{\nu}) \cdot I_{pump}(t, \tilde{\nu})$ and $k_{ji} = k_{ij}\frac{N_i}{N_j}$ are coupled by detailed balance. $I_{pump}(t, \tilde{\nu})$ is the IR_{pump} laser intensity profile which was assumed to be Gaussian with 20 ps FWHM. The right panel of Fig. A3 shows the resulting fractional population distributions over different manifolds, E_i, obtained at

two laser fluences: 0.014 (black) and 0.031 J/cm^2 (blue). These values realistically represent the two pump laser fluences shown in Fig. 2c.

To obtain a simulation of the experimentally determined SFG spectra, the IR_{pump} induced SFG spectrum was calculated by generalizing Eq. (2) to allow for a manifold of resonant transitions.

$$I_{SFG} \propto \left| \left|\chi_{Au}^{(2)}\right| + \sum_i \left(\sum_j \frac{a_j\, e^{-i\varphi_j}}{(\omega_j - \omega - i\Gamma_j)} + \sum_k \frac{a_k\, e^{-i\varphi_k}}{(\omega_k - \omega - i\Gamma_k)} \right) \right|^2 \tag{A14}$$

Where the double sum is over all exciton manifolds *i* containing transitions *j* with v=0↔1 and *k* with v=1→2 character. Here,

$$a_j = \bar{\sigma}_j \cdot \left(\frac{P_i}{N_i} - \frac{P_{i+1}}{N_{i+1}} \right), \tag{A15}$$

accounts for absorption and simulated emission where as

$$a_k = \bar{\sigma}_k \cdot \frac{P_i}{N_i}\,. \tag{A16}$$

does not require stimulated emission.

The phase factors in Eq. A14 have a crucial effect on the observed SFG spectra. We have modeled them as follows. All phases for 0→1 and 1→2 transitions are assumed identical, respectively, and $\varphi_k = \varphi_{12}$ is shifted by $\approx -110°$ with respect to φ_{01}. Only then can we produce a destructive interference with the non-resonant contribution that leads to a realistic simulation of the data in Fig. 2cNote that all phases are shown relative to the Au-plasmon related non-resonant phase, which was globally set to zero.

Fig. A4 shows the resulting SFG spectra (upper panel) calculated in this way and the S_{pump}/S_0 ratio (lower panel) shown in Fig. 2c. The black curve in the upper panel is the reference spectrum with no vibrational excitation of CO. It coincides with the fitted spectrum of Fig 2b. The blue spectrum results for model conditions corresponding to the black points in the right panel of Fig. A3, a realistic simulation of our 30 μJ pulse-energy data shown in Fig. 2c. It corresponds to 10% of the CO molecules being pumped to v=1.

The ratio of the two spectra S_{pump}/S_0 presented in the lower panel of Fig. A4 (blue curve) shows two features with reduced (2104 and 2131 cm^{-1}) and one with enhanced intensity (2135 cm^{-1}) in agreement with the experiment. All the amplitudes increase with the degree of 0→1 excitation. The amplitude of the 2131 cm^{-1} feature, however, also depends on the energy dependent red-shift of the exciton bands (see Fig. A2). This shift depends on the coupling strength, which allows for tuning the amplitude ratio of the features at 2104 and 2131 cm^{-1}. In this way, the agreement to the experimental data was improved by adjusting the

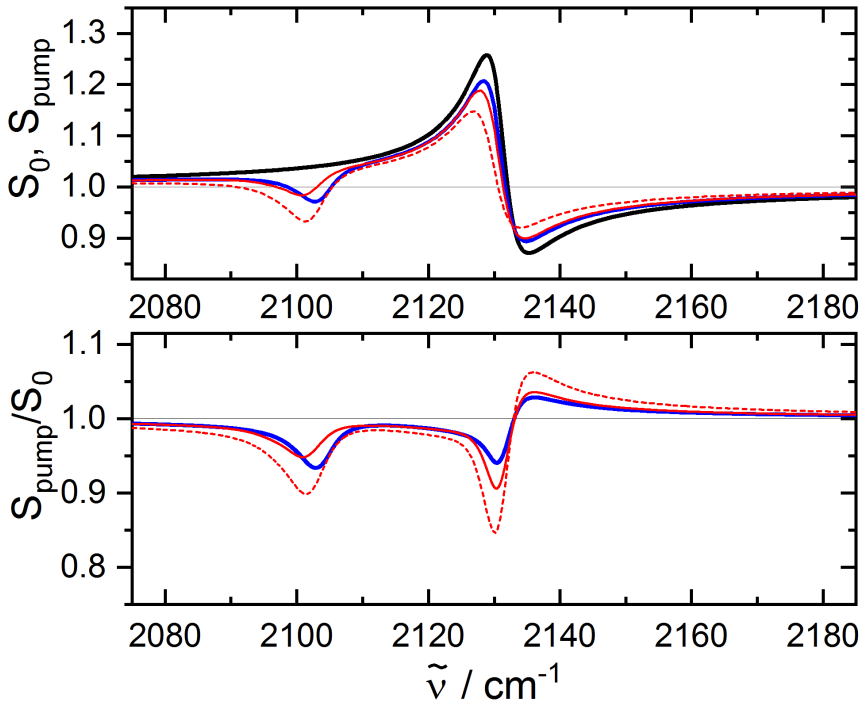

Figure A4. Upper panel: Calculated SFG spectra without vibrational excitation (black) and with 10% (blue and red solid lines) and 20% (red dashed line) of CO molecules excited by the pump pulse. For the blue curve the gas-phase dipole and transition dipole moments were used, for the red curves the gas phase dipole moments where scaled by a factor 0.2 and the transition dipole moments by a factor 1.5. Lower panel: The pump pulse induced changes normalized to the static SFG spectrum. All spectra were generated with a common line width of $\Delta\tilde{\nu} = 6\ cm^{-1}$.

dipole matrix elements. In Fig. A4 the red curves are obtained for 10% (solid) and 20% (dashed) fractional excitation of the CO molecules by scaling μ^{00}, μ^{11}, and μ^{22} with a factor 0.2 and the transition dipole moments μ^{01} and μ^{12} with a factor of 1.5.

To summarize, we have presented a realistic model of our SFG spectra that reproduces the most important features of the observed spectra. While some questions remain – e.g. why φ_{12} must be shifted by $\approx -100°$ with respect to φ_{01} – we believe the assignments of spectral features are correct. Ultimately this is all that is needed to determine the vibrational lifetime.

VIBRATIONAL LIFETIME MODEL FOR A PHYSISORBED MOLECULE

Persson and others [9-12] have calculated the damping of a vibrating dipole in the presence of a metal surface at a distance *d*. In Ref. [11] it is shown that for molecules interacting weakly with the metal - conditions which can be considered as physisorption - the relaxation for $d < 100$ Å is dominated by the near and induction fields from the molecule, which transfer energy to the metal's electrons. In Fig. 5 of Ref.

[11] the calculated vibrational lifetime τ is shown vs. the reduced distance $d \cdot k_F$, where k_F is the Fermi wave vector, for a molecule with a vibrational frequency of ν=2016 cm^{-1} and a transition dipole moment of 0.1 D adsorbed on a metal with a Wigner-Seitz radius of r_s = 2 a.u.. Since τ is proportional to r_s and $1/\nu$ this curve can be easily scaled and then used to predict lifetimes of CO/Au(111) (transition dipole moment of 0.1 D, ν=2132 cm^{-1} and r_s = 3.01 a.u. [13]). We use the Fermi wave vector of Au, k_F(=1.2·10^{10} m^{-1})[13], to obtain $\tau(d)$ as shown in the following figure.

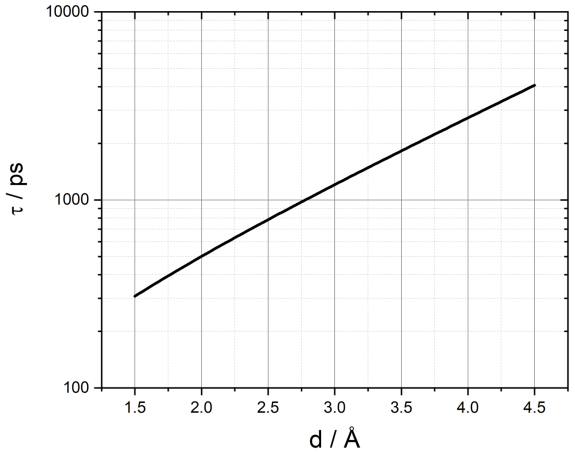

Fig. A5: Calculated vibrational lifetime of CO/Au(111).

While this theory indeed shows that the lifetime of a physisorbed CO molecule on Au(111) is expected to be longer than that of a chemisorbed CO molecule, the predicted lifetimes are much longer than observed in our work. A recent DFT calculation of the binding distance of physisorbed CO on Au(111) using a BEEF-vdW functional gave 3.7-4 Å [14], suggesting a lifetime of 2-3 ns. Even at shorter distances, the lifetime is longer than observed in experiment.

This analysis depends on an assumption about the CO adsorbate structure, which is not fully known. Specifically, we have assumed that the CO bond is parallel to the surface normal. Some independent information about the structure is available from Gajdos et al., who report a DFT investigation of CO adsorption on close packed noble and transition metal surfaces, including Au(111) [8]. They report on the c(2x4) overlayer (0.25 ML) with CO on the top site oriented vertically. These structures have been verified experimentally for Ni(111) and Pt(111) but not yet for Au(111). In another theoretical study, Maurer et al. assumed a p(2x2) structure for CO on Au(111) [15]. These theoretical treatments all yield a CO bond parallel to the surface normal.

References to the Appendix

[1] R. Disselkamp, H.-C. Chang, and G. E. Ewing, Surf. Sci. **240**, 193 (1990).

[2] D. J. Dai and G. E. Ewing, Surf. Sci. **312**, 239 (1994).

[3] S. Woutersen and P. Hamm, J. Phys.: Condens. Matter **14**, R1035 (2002).

[4] A. S. Davydov, *Theory of Molecular Excitations* (Plenum, New York, 1971).

[5] P. Hamm, M. Lim, and R. M. Hochstrasser, J. Phys. Chem. B **102**, 6123 (1998).

[6] H.-J. Werner, Mol. Phys. **44**, 111 (1981).

[7] H.-J. Chen, J. Wu, H. Liu, and X.-L. Cheng, Chin. Phys. B **24**, 083102 (2015).

[8] M. Gajdoš, A. Eichler, and J. Hafner, Journal of Physics: Condensed Matter **16**, 1141 (2004).

[9] B. Persson, J. Phys. C: Solid State Phys. **11**, 4251 (1978).

[10] B. N. J. Persson and S. Andersson, Phys. Rev. B **29**, 4382 (1984).

[11] B. N. J. Persson and M. Persson, Surface Science **97**, 609 (1980).

[12] A. Liebsch, Physical Review Letters **54**, 67 (1985).

[13] C. Kittel, *Introduction to solid state physics* (Wiley, 2005), 8th edn.

[14] I. Loncaric, M. Alducin, J. I. Juaristi, and D. Novko, J. Phys. Chem. Lett **10**, 1043 (2019).

[15] R. J. Maurer, M. Askerka, V. S. Batista, and J. C. Tully, Physical Review B **94**, 115432 (2016).